
X-Ray induced fluorescence measurement of segregation in a DyI₃-Hg metal-halide lamp.

Abstract. Segregation of elemental Dy in a DyI₃-Hg metal-halide high-intensity discharge lamp has been observed with x-ray induced fluorescence. Significant radial and axial of Dy segregation are seen, with the axial segregation characterized by a Fischer parameter value of $\lambda = 0.215 \pm 0.002 \text{ mm}^{-1}$. This is within 7% of the value ($\lambda = 0.20 \pm 0.01 \text{ mm}^{-1}$) obtained by Flikweert *et al* (J. Appl. Phys. **98** 073301 (2005)) based on laser absorption by neutral Dy atoms. Elemental I is seen to exhibit considerably less axial and radial segregation. Some aspects of the observed radial segregation are compatible with a simplified fluid picture describing two main transition regions in the radial coordinate. The first transition occurs in the region where DyI₃ molecules are in equilibrium with neutral Dy atoms. The second transition occurs where neutral Dy atoms are in equilibrium with ionized Dy. These measurements are part of a larger study on segregation in metal-halide lamps under a variety of conditions.

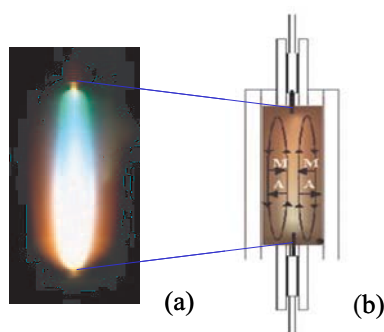


Figure 6.1: (a) Colour separation in a metal-halide lamp burner caused by axial segregation. (b) Schematic view of a metal-halide lamp; diffusion and convection of atoms (A) and molecules (M) are indicated by arrows. See figure 1.1 for full colour.

6.1 Introduction

Metal-halide lamps are compact, high-intensity light sources with high luminous efficacy and good colour rendering [1]. They consist of an electric discharge through a high-pressure Hg vapour containing a relatively small amount of additives consisting of metal-halide salts. Two or more salts are typically used to maximize the colour rendering index. Mixtures such as $(\text{NaI} + \text{ScI}_3)$, $(\text{NaI} + \text{TlI} + \text{InI})$ or $(\text{NaI} + \text{TlI} + \text{DyI}_3 + \text{HoI}_3 + \text{TmI}_3)$ are common in commercial lamps. Although the additives are present in densities much smaller than that of Hg, they dominate the ionization and power balances of the discharge because they have excitation and ionization potentials much lower than those of Hg. At operating temperatures, metal-halide molecules diffuse into the Hg vapour where they are dissociated to varying degrees depending on the local temperature. In the core of the arc, where temperatures are highest, the additive metal-halides are completely dissociated and even partially ionized. Excitation of additive metal atoms and ions in the core of the discharge is the primary source of visible radiation from these lamps.

The spatially inhomogeneous distribution of atomic and molecular species in metal-halide arcs can combine with complex transport mechanisms to produce an effect called segregation, or de-mixing [2]. Segregation refers to a non-uniform distribution of additives relative to the Hg buffer gas. It can lead to deficiencies in colour uniformity (see figure 6.1) and a reduction in luminous efficacy. In order to gain a better understanding of the segregation phenomena, we have used x-ray induced fluorescence [3, 4] to measure the spatial distributions of both the additives and the Hg in a test lamp specifically designed to enhance segregation.

The lamp type in question has been studied previously by Nimalasuriya *et al* [5] using optical techniques, yielding density distributions of atomic and ionic species of the additives and Hg. This technique, however, does not provide molecular densities and requires extensive data analysis. The lamp was also studied using laser absorption [6], which yields only the density of Dy in its ground state. In the present study, x-ray induced fluorescence

was used to directly measure elemental densities. Elemental density includes the contribution of the ions, atoms and molecules. X-ray induced fluorescence consists of irradiation of an atom using photons with energy sufficient to eject an inner shell electron. X-ray fluorescence, with energy characteristic of the atomic number of the atom, is emitted when an outer shell electron fills the inner shell vacancy created by the incident photon. This technique allows for a direct measurement of elemental density independent of the state of the atom such as excitation, ionisation or molecular bonding.

Previous x-ray induced fluorescence measurements of a metal halide lamp were made by Curry *et al* [3] on a ceramic metal halide lamp of a different burner geometry and filling. The lamp type used in the present study was previously observed under both reduced and enhanced gravity [7, 8, 10, 11] and studied by x-ray absorption techniques [12]. The lamp was filled with a Hg buffer gas and one salt, namely DyI₃. The simplicity of this salt system makes it easier to compare measurements with results of a numerical model.

6.2 Theory

Only a small fraction of the DyI₃ salt evaporates and enters the discharge, leaving a liquid salt pool at the coldest spot of the burner wall. The temperature of the liquid salt pool determines the vapour pressure of the additive in the vicinity of the cold spot. The temperature of the arc, which varies from more than 6000 K in the core to less than 1200 K near the wall [12], leads to varying degrees of dissociation, and even ionization, of the evaporated additive. Here we signify species produced by varying states of dissociation and ionization by a subscript i and the number density of a particular species by n_i . Elements are signified by a subscript in braces $\{\alpha\}$. The number density of a particular element, $n_{\{\alpha\}}$, is the sum over all species containing that element

$$n_{\{\alpha\}}(r, z) = \sum_i R_{i\{\alpha\}} n_i(r, z). \quad (6.1)$$

where R is the stoichiometric coefficient.

The distributions of elemental densities are influenced by three principal factors. First, the gas temperature affects densities through partial pressures

$$p_{\{\alpha\}} = n_{\{\alpha\}}(r, z)kT(r, z) = \sum_i R_{i\{\alpha\}} n_i(r, z)kT(r, z). \quad (6.2)$$

where k is Boltzmann's constant and $T(r, z)$ is the heavy particle temperature. It is assumed that the latter is identical to the chemical equilibrium temperature. It may also coincide with the electron gas temperature, the atomic/molecular excitation temperature, or radiation temperature in certain regions of the discharge. The spatial distribution of $T(r, z)$, which peaks on the arc axis, produces a heavy particle distribution which has a minimum on the axis.

Second, the distributions of elemental densities are influenced by radial segregation. This effect is produced by the different radial diffusion velocities of different atomic and

molecular species. Ambipolar diffusion [13], in particular, causes ions to diffuse out of the core faster than neutral atoms or molecules diffuse inward. A steady-state can only be achieved when the elemental density of Dy is lower in the core than it would be in the absence of the difference in diffusion velocities [3].

Third, the distributions of elemental densities are influenced by axial segregation, an effect produced by a combination of radial diffusion and gravity-driven axial convection. It usually leads to an accumulation of radiating additives near the bottom of the arc, sometimes with a significant impact on the colour uniformity (figure 6.1). Fischer characterised axial segregation with a parameter λ such that [2]:

$$p_{\{\alpha\}}(z) = p_{\{\alpha\}}(0) \exp(-\lambda_{\{\alpha\}}z), \quad (6.3)$$

where z is the axial position relative to the tip of the lower electrode. $\lambda_{\{\alpha\}}$ is called the segregation parameter for the element α . Since densities, and not partial pressures, are measured experimentally, it is useful to reformulate equation 6.3 in terms of the mixing ratio, $n_{\{\alpha\}}/n_{\{Hg\}}$. Dividing equation 6.3 by the total lamp pressure $p_0 \approx n_{\{Hg\}}(r, z)kT(r, z)$, which is not a function of position, gives

$$\frac{n_{\{\alpha\}}(z)}{n_{\{Hg\}}(z)} = \frac{n_{\{\alpha\}}(0)}{n_{\{Hg\}}(0)} \exp(-\lambda_{\{\alpha\}}z). \quad (6.4)$$

Here, the r -dependence has been suppressed because the Fischer model is one-dimensional. In a well-mixed system, $\lambda_{\{\alpha\}} = 0$ for all additives, i.e. the mixing ratios do not depend on z , even if $n_{\{\alpha\}}$ and $n_{\{Hg\}}$ do. Spatial variations in the mixing ratios signify segregation.

Three principal regions can be identified within the radial density distribution of elemental Dy (see figure 6.2). These are 1) the region near the wall where DyI_3 molecules are predominant, 2) the mantle region between the wall and the arc core where Dy atoms predominate, and 3) the core where the Dy is almost completely ionized in the form of Dy^+ . The molecules DyI_2 and DyI are relatively unstable and do not have a dominant presence in any region of the discharge [15].

It is interesting to examine the balance of radial fluxes of the additive elements and the resulting behaviour of elemental density distributions at the two transitions between these regions. Following Hartgers *et al* [14], the radial flux $\Gamma_{\{\alpha\}}$ of element α can be written

$$\Gamma_{\{\alpha\}} = \sum_i R_{i\{\alpha\}} \left[-\frac{D_i}{kT} \frac{\partial p_i}{\partial r} + \frac{p_i}{kT} u_r + \frac{D_i}{kT} \frac{q_i}{q_e} \frac{p_i}{p_e} \frac{\partial p_e}{\partial r} \right]. \quad (6.5)$$

The summation in equation 6.5 is over each species i containing element α and e refers to the electron population. The diffusion coefficient, D_i , characterizes diffusion of species i through the Hg vapour; elastic collisions with other species are ignored because of the low density of other species compared to Hg. u_r is the radial convective flow and q designates charge. The first term on the right hand side of equation 6.5 represents the diffusion of species due to partial pressure gradients. The second term on the right hand side represents the flux arising from convective flow. Although, as mentioned earlier, axial convective flow can give rise to segregation, in analyzing radial segregation we will ignore the radial

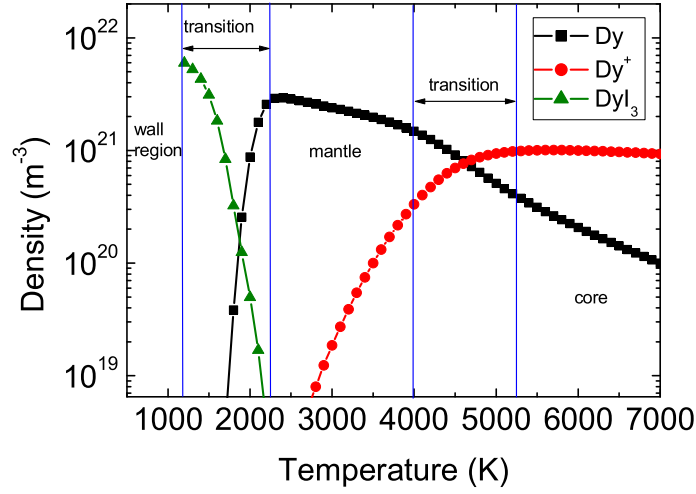


Figure 6.2: Theoretical density distribution of Dy atoms, ions and molecules as a function of temperature at the midplane of a metal-halide lamp containing $2 \cdot 10^6$ Pa (20 atm) of Hg. For clarity, DyI_2 and DyI have been omitted. (courtesy to M L Beks)

convective flow, u_r . Finally, the third term on the right hand side describes ambipolar diffusion of the charged species and arises from the relatively rapid movement of electrons outward from the core and the subsequent charging of the core, which in turn, produces the ambipolar electric field. Hereafter we will assume that for the relevant regions the different forms of radial transport must balance so that in these transition regions the net flux of each element vanishes i.e.,

$$\Gamma_{\{\alpha\}} = 0. \quad (6.6)$$

The transition region between the wall and mantle is characterized by the reaction



The tri-iodide molecule is stable in the region closest to the wall and diffuses inward as a result of a positive partial pressure gradient, while the atomic species are stable in the mantle region and diffuse outward due to a negative partial pressure gradient. Ions and electrons have negligible densities at this transition. Therefore ambipolar diffusion is not significant here. Equation 6.5 gives for Dy

$$\Gamma_{\{\text{Dy}\}} = - \left(\frac{D_{\text{DyI}_3}}{kT} \right) \frac{\partial p_{\text{DyI}_3}}{\partial r} - \left(\frac{D_{\text{Dy}}}{kT} \right) \frac{\partial p_{\text{Dy}}}{\partial r} = 0. \quad (6.8)$$

Assuming the ratio of diffusion coefficients is constant, equation 6.8 can be integrated over the transition region to yield

$$p_{Dy}|_h = \left(\frac{D_{DyI_3}}{D_{Dy}} \right) p_{DyI_3}|_c \quad (6.9)$$

where c and h refer to the hot and cold side of the transition region. Using $n_{Dy}|_h \approx n_{\{Dy\}}|_h$ and $n_{DyI_3}|_c \approx n_{\{Dy\}}|_c$, and employing $p_i = n_i kT$ this can be rewritten as

$$\frac{n_{\{Dy\}}|_h}{n_{\{Dy\}}|_c} \approx \left(\frac{D_{DyI_3}}{D_{Dy}} \right) \frac{T_c}{T_h}. \quad (6.10)$$

Equation 6.10 suggests that the density of elemental Dy will change across this transition region by the factor, $\left(\frac{D_{Dy}}{D_{DyI_3}} \right) \approx 3$. That is, radial segregation of a factor of three is expected just inside the discharge wall, simply because the tri-iodide molecule diffuses more slowly than the Dy atom. The same argument holds for the other rare-earth tri-iodides commonly used in metal-halide lamps.

The same analysis for I across this transition does not suggest radial segregation because, although the tri-iodide molecule diffuses approximately three times more slowly than the I atoms, the molecule carries three times as many I atoms.

The second transition region, between the mantle and the core, is characterized by the reaction



Here, Dy atoms are stable in the outer, cooler region and diffuse inward as the result of a positive partial pressure gradient, while Dy ions are stable in the core and diffuse outward as the result of a negative partial pressure gradient. In addition, Dy ions are subject to the ambipolar field, which enhances their diffusion out of the core. The balance of fluxes at this transition is

$$\left(\frac{D_{Dy}}{kT} \right) \frac{\partial p_{Dy}}{\partial r} + \left(\frac{D_{Dy^+}}{kT} \right) \frac{\partial p_{Dy^+}}{\partial r} + \left(\frac{D_{Dy^+}}{kT} \right) \frac{p_{Dy^+}}{p_e} \frac{\partial p_e}{\partial r} = 0. \quad (6.12)$$

In the lamp used for the present study, where segregation is severe and the density of Dy in the core is not sufficient to lower the core temperature significantly from what is seen in a pure Hg discharge [5,7], the electron density can be replaced in the preceding equation by the Hg ion density, i.e., $p_e \approx p_{Hg^+}$. Rewriting equation 6.12 in terms of elemental densities yields

$$D_{Dy} n_{\{Hg\}} \frac{\partial}{\partial r} \left(\frac{n_{Dy}}{n_{\{Hg\}}} \right) + D_{Dy^+} n_{\{Hg\}} \frac{\partial}{\partial r} \left(\frac{n_{Dy^+}}{n_{\{Hg\}}} \right) = -D_{Dy^+} n_{\{Hg\}} \frac{n_{Dy^+}}{n_{Hg^+}} \frac{\partial}{\partial r} \left(\frac{n_{Hg^+}}{n_{\{Hg\}}} \right). \quad (6.13)$$

Assuming $D_{Dy} \approx D_{Dy^+}$ and $n_{Dy} + n_{Dy^+} = n_{\{Dy\}}$ in this region, the two terms on the left hand side of equation 6.13 can be combined,

$$[D_{Dy} n_{\{Hg\}}] \frac{\partial}{\partial r} \left(\frac{n_{\{Dy\}}}{n_{\{Hg\}}} \right) = - [D_{Dy} n_{\{Hg\}}] \frac{n_{Dy^+}}{n_{Hg^+}} \frac{\partial}{\partial r} \left(\frac{n_{Hg^+}}{n_{\{Hg\}}} \right). \quad (6.14)$$

The term on the left hand side represents the flux arising from partial pressure gradients, while the term on the right hand side represents the flux arising from ambipolar diffusion. Although there is no simple analytic integration of equation 6.14, the terms on each side of the equation may be evaluated using experimental data. Elemental densities have been measured in the present work with x-ray induced fluorescence, while the Hg and Dy ion densities have been measured with optical emission spectroscopy [5, 7].

6.3 The experiment

6.3.1 The Lamp

The lamp we examined was designed to maximize segregation in order to facilitate the study of this effect. Observations of this and other lamps designed for the same purpose have been reported previously [6, 6, 12], including observations under micro- and hyper-gravity conditions [7, 8]. The lamp consists of an 8 mm inner diameter quartz arc tube surrounded by a quartz outer vacuum jacket. The electrode gap is 18 mm. The lamp contains 10 mg of Hg and 3.7 mg of DyI₃ [15]. For the measurements presented here, the lamp was operated vertically at a power of 145 W. Power was supplied by an electronic square-wave ballast at a frequency of 122 Hz. The lamp voltage and current waveforms were monitored with a digital oscilloscope and lamp power was calculated from their time-averaged product. The latter was stable to better than 1%.

6.3.2 X-ray induced fluorescence

Use of x-ray induced fluorescence (XRF) to obtain spatially-resolved, absolute densities of additives in metal-halide lamps has been described by Curry *et al* [3]. This method measures elemental density, the density of a particular element summed over all atomic and molecular species. It is therefore able to directly observe mixing ratios without resorting to assumptions about partition functions. We measured the elemental densities of fluorescence at the Sector 1 Insertion Device beam line at the Advanced Photon Source, Argonne National Laboratory [16]. A beam of monochromatic, high-energy photons (70 keV or 86 keV) was used to excite fluorescence in the arc constituents. The incoming photon flux was measured by a nitrogen-filled ionization chamber and the fluorescence photons were detected with an energy-resolving Ge detector situated to observe photons emitted in a direction perpendicular to the incident beam. The energy response of the detector is flat from approximately 20 keV to approximately 80 keV, falling off by only about 15% between 80 keV and 100 keV.

Spatial resolution was obtained by using a small beam cross section (0.5 mm wide by 1.0 mm high) and restricting the field of view of the detector to a small length of the incident beam (figure 6.3) using a 500 μm diameter pinhole aperture and the 11.3 mm diameter aperture of the detector. Absolute calibration of densities was obtained by comparing fluorescence intensities from Dy, I, and Hg in the lamp described above with fluorescence

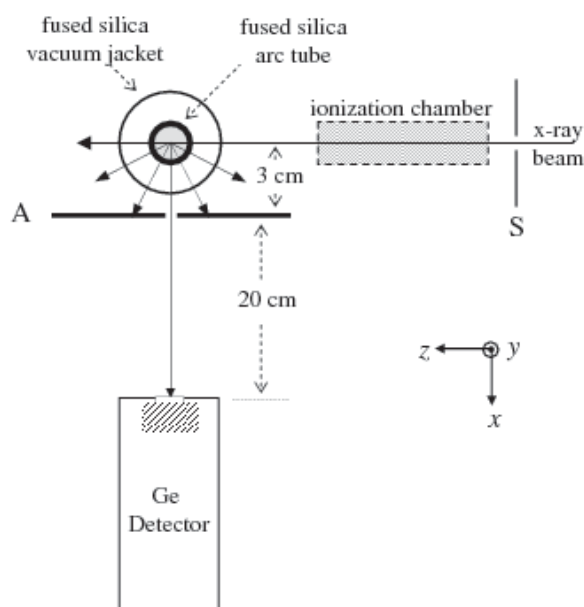


Figure 6.3: Experimental setup for x-ray induced fluorescence in a metal-halide lamp. The x-ray beam is extracted from the Sector 1 Insertion Device beam line at the Advanced Photon Source.

intensity from a cell containing a known density of Xe atoms.

The density of Hg was obtained using an incident photon energy of 86 keV. The small cross-sections for excitation of Dy and I at this energy and the much stronger signal from Hg made it difficult to measure the much lower densities of the additives with good signal-to-noise. The densities of Dy and I were observed, instead, with an incident photon energy of 70 keV, where the cross-sections of the additives are larger and Hg fluorescence is not excited. The two sets of data were acquired on slightly different radial spatial grids, so mixing ratios are computed using Hg densities obtained from radial polynomial fits to the Hg data.

The densities of the additives were corrected for absorption of fluorescence by Hg atoms. This correction is most significant for I because of its lower energy fluorescence, but never exceeds 12%. For Dy, it never exceeds 4%.

A spectrum taken near the bottom electrode at a beam energy of 70 keV is shown in figure 6.4; it clearly shows Dy and I peaks. Ce fluorescence peaks are also seen. Ce is present in the lamp vacuum jacket and multiple photon scattering events allow it to be seen by the detector.

6.4 Results and Discussion

Elemental densities for Hg, Dy, and I are shown in Figures 6.5, 6.6, and 6.7. The error bars in these figures indicate typical random uncertainties. For both Hg and I, relative

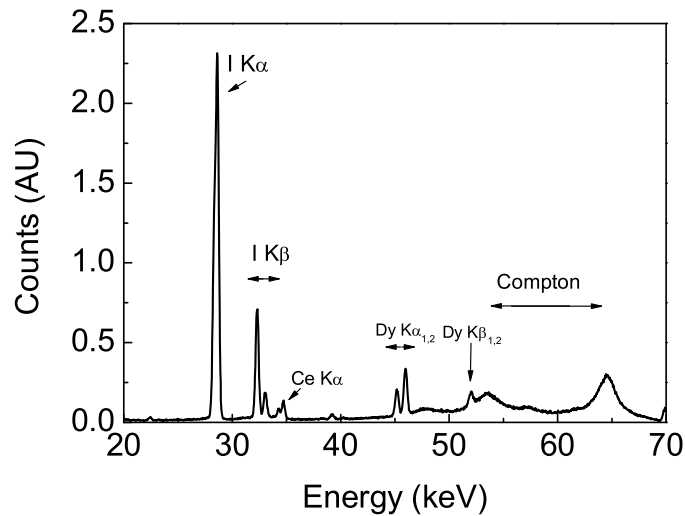


Figure 6.4: X-ray induced fluorescence spectrum excited by 70 keV photons at $x/R = 0.3$, where x is the displacement from the arc axis in the direction of the detector and $R = 0.004$ m is the radius. The horizontal arrow indicates the spectral range of broad peaks due to Compton scattering by the arc tube and vacuum jacket. Counts are given in arbitrary units.

random uncertainties are less than 1% and the error bars are too small to be seen clearly on the scale of the figures. The random component of uncertainty in the present case is due entirely to the precision with which a baseline can be determined for the fluorescence peaks and is influenced by both random detector noise and by any interfering spectral feature. Although the latter might be more properly considered a systematic uncertainty, at least for a given data point, it is much more natural to assign to the same category as detector noise.

Systematic uncertainties in x-ray fluorescence measurements of this kind are discussed in [4]. In dealing with plasma systems, it is rarely worth the effort to make absolute measurements with uncertainties of less than 5% because plasmas are seldom reproducible at a higher level. For the present discussion, we emphasize the density of elemental components relative to each other, a process that eliminates many of the possible systematic errors. The ratio of Dy to I at a given location, for example, is derived from a single spectrum in which all features are acquired simultaneously.

Comparison of Xe calibration spectra and of I fluorescence intensities acquired at the two different excitation energies indicates that the efficiency of our fluorescence collection system changed at some point during data acquisition at high energy, most likely as a result of the detector being bumped. Normally, a small movement of the detector is not important because it is under-filled. In this case, however, it was a limiting aperture. Any movement of the detector must have occurred between data runs, because the experimental chamber is

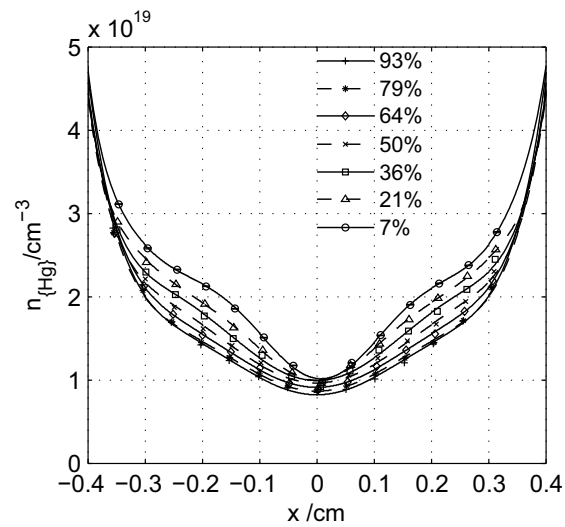


Figure 6.5: Radial profiles of elemental Hg at different axial positions. The axial positions are given as a percentage of the total length of the arc relative to the lower electrode.

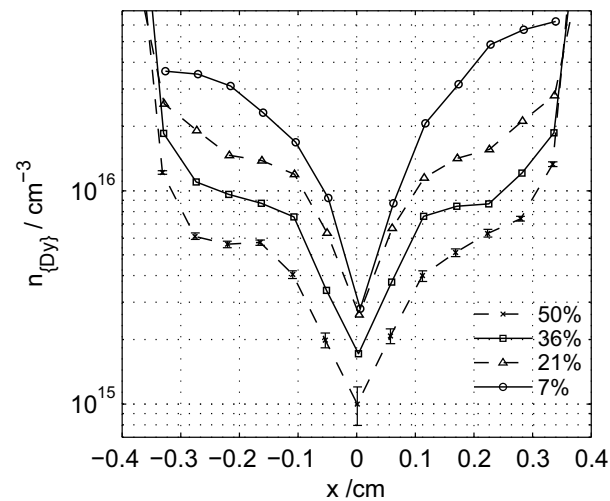


Figure 6.6: Radial profiles of elemental Dy at different axial positions. The axial positions are given as a percentage of the total length of the arc relative to the lower electrode.

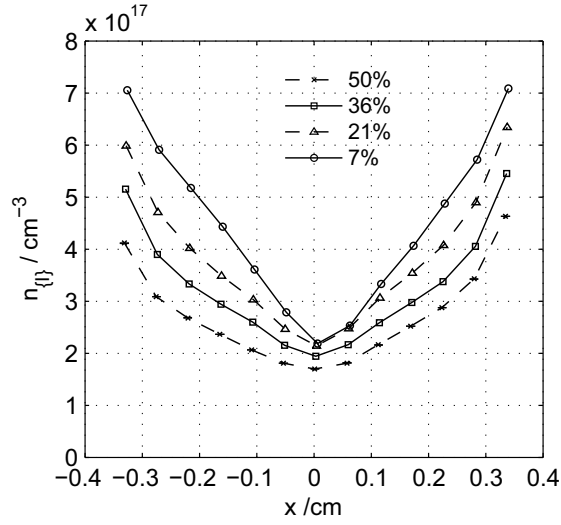


Figure 6.7: Radial profiles of elemental I at different axial positions. The axial positions are given as a percentage of the total length of the arc relative to the lower electrode.

inaccessible during data acquisition. Therefore, spatial distributions and relative intensities are not affected. In addition, we have scaled the measurements at high energy to match those at low energy using the iodine fluorescence, which was adequately strong in both cases. This gives an estimated systematic uncertainty of $\pm 20\%$.

The measured Hg densities in figure 6.5 have been fit to radial polynomials. The fitted radial profiles are extended to the discharge wall by using wall densities obtained by combining pyrometrically-measured wall temperatures from Zhu, T_{wall} , [12] and an estimated lamp pressure of $p_0 = 8 \times 10^5$ Pa (8 atmospheres) to obtain $n_{\{Hg\}}(wall) = p_0/kT_{wall}$. The Hg density shows a clear constriction of the arc core (high temperature region) in the vicinity of the lower electrode and a steady decrease in density as one moves upward, indicative of increasing temperature with increasing height. The primary cause of the constricted core at the bottom of the arc is the presence of Dy atoms and ions. The broad optical emission spectra of Dy atoms and ions efficiently radiate power, thereby cooling the arc core and causing the arc to constrict [17]. On the other hand, axial segregation has considerably reduced the Dy density at points higher in the arc, as will be seen in figure 6.6. Constriction near the lower electrode was also observed in this lamp design using optical emission [5, 7].

Zhu [12] measured the Hg density in a nominally identical lamp under similar conditions using x-ray absorption imaging. She did not publish the Hg density data, but instead published temperature profiles, T_{Zhu} , derived from that data. Using her reported lamp pressure of $p_0 = 10 \times 10^5$ Pa (10 atmospheres), we compare p_0/kT_{Zhu} with our own measured Hg densities in Figures 6.8 and 6.9. Radial distributions near both the upper and the lower electrode are shown. Our measurements are generally about 40% lower than that implied by Zhu. The narrow core is also better resolved by x-ray induced fluorescence than by x-ray

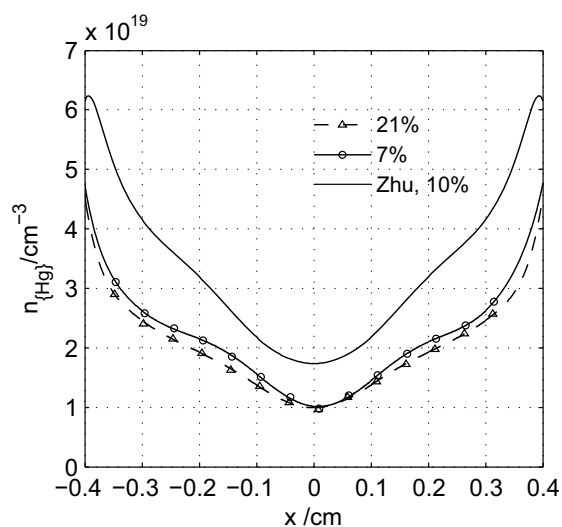


Figure 6.8: Comparison of elemental Hg densities with measurements made by Zhu [12] using x-ray absorption imaging. Axial positions are given as a percentage of the total length of the arc relative to the lower electrode.

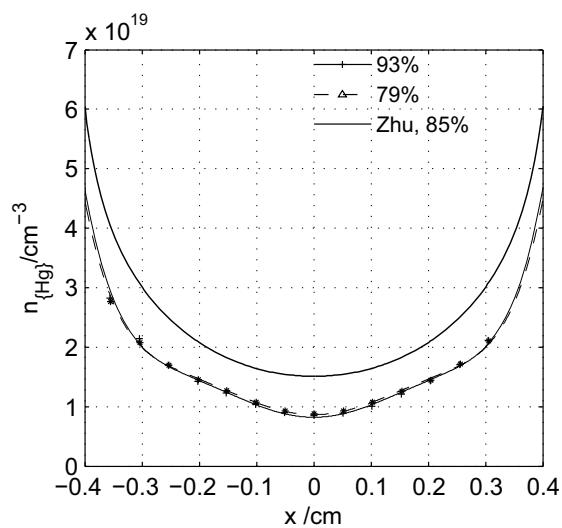


Figure 6.9: Comparison between Hg densities measured with x-ray induced fluorescence and densities measured with x-ray absorption imaging by Zhu [12]. Axial positions are given as a percentage of the total length of the arc relative to the lower electrode.

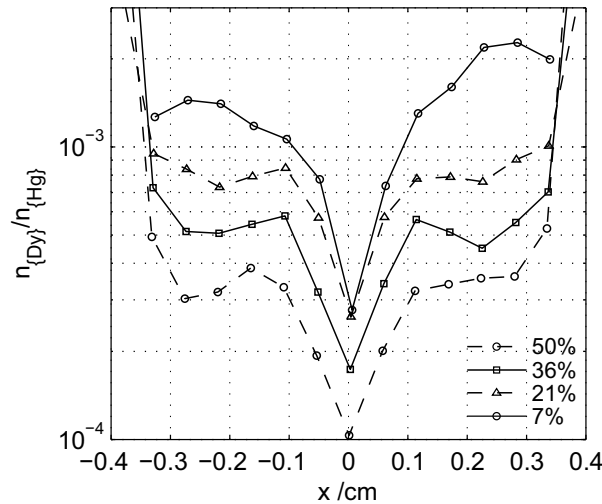


Figure 6.10: The mixing ratio $n_{\{Dy\}}/n_{\{Hg\}}$, with the axial positions given as a percentage of the total length of the arc relative to the lower electrode.

absorption imaging. Although x-ray absorption imaging, in principle, has better spatial resolution, it can be limited in practice by the need to reduce measurement noise that would be unacceptably amplified by the Abel inversion.

The measured elemental Dy densities (see figure 6.6) are of the same order of magnitude as seen in laser absorption measurements of the neutral atomic ground state densities obtained by Flikweert *et al* [6] in a nominally identical lamp, in the region where neutral atomic Dy is the dominant Dy species.

The measured elemental I densities (see figure 6.7) are on the order of 100 times larger than the Dy densities. Two causes are suggested for this large factor. First, the segregation of Dy is extremely large because the experimental lamp was designed to maximize this effect. Second, both x-ray fluorescence measurements with the lamp off and a post-experiment chemical analysis confirm the formation of Dy-silicates on the arc tube. The permanent removal of Dy from the discharge leaves an excess of free I.

The Dy mixing ratio as a function of both radial and axial position is shown in figure 6.10. There are two distinct transition regions in the radial profiles, corresponding to the transition regions discussed in Section 6.2. Near the wall, the mixing ratio drops precipitously for three of the four profiles. This corresponds to the transition from DyI_3 molecules near the wall to Dy atoms in the mantle. The simple theoretical model discussed in Section 6.2 suggested a factor of three drop in the mixing ratio across this transition. Three of the four profiles show a much larger drop, while the lowest profile shows a smaller drop. At least some of the larger drop for the upper profiles in the Dy mixing ratio is attributable to the permanent accumulation of Dy on the wall in the form of Dy-silicates. In other words, measurements made at the wall contained some contribution from the much higher density of Dy attached to the wall. Visual inspection indicated that accumulation

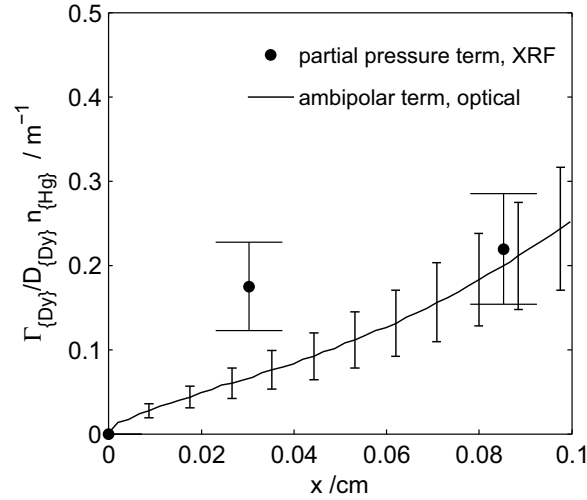


Figure 6.11: The radial gradients giving rise to the Dy elemental flux density (see equation 6.14) in the core of the arc at the midplane are evaluated. The partial pressure term (left hand side of equation 6.14) is evaluated with the x-ray induced fluorescence measurements presented here, while the ambipolar term (right hand side of equation 6.14) is evaluated with data from optical emission measurements [5, 7].

of Dy silicates on the wall was considerably less at the height of the lower electrode and below, presumably as a result of lower wall temperatures. For the lowest radial profile in figure 6.10, partial overlap of the x-ray beam with the wall at the largest radial values would reduce the measured Dy density, rather than increase it, as would be the case at higher axial positions. A clear distinction between the wall and the transition region where Dy molecules are dissociated requires a finer spatial resolution than we used.

The second distinct transition region occurs at the edge of the core. The Dy mixing ratio decreases by a factor of 3 or more over this transition. Here we used our measured Dy mixing ratio to evaluate the gradient in the partial pressure flux density term on the left-hand side of equation 6.14. We also used published measurements of n_{Hg^+} and n_{Dy^+} densities from optical emission observations [5, 7] to evaluate the gradient in the ambipolar flux density term on the right hand side of equation 6.14. These latter measurements were acquired in a lamp of the same design as the one used here, although at a lower power of 100 W. This difference in operating power could significantly affect the cold spot temperature and therefore the amount of Dy in the arc. The results are shown in figure 6.11 for the core region ($r \leq 1$ mm, where equation 6.14 is expected to be valid) in the midplane of the arc. In this limited range of r , there are only two data points from the x-ray induced fluorescence measurements. Considering the different operating powers under which the two data sets were obtained, the agreement between the two flux terms is surprisingly good. The comparison near $r = 0.8$ mm shows excellent agreement between the partial pressure gradient flux term and the ambipolar flux term, while the comparison near $r = 0.3$ mm shows the partial pressure flux term to be approximately twice as large as the ambipolar

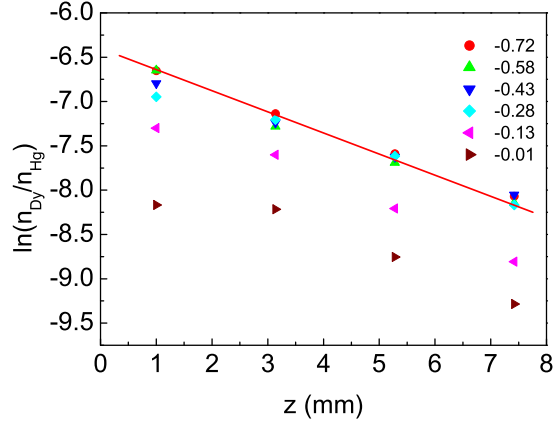


Figure 6.12: Natural logarithm of the Dy mixing ratio versus axial position, z , for several radial positions. The tip of the lower electrode is located at $z = 0$ mm. The radial positions are given as a fraction of the full radius of the arc tube. The straight line is a fit to data at a normalized radius $x/R = 0.72$.

term. A more thorough study of the radial fluxes in the core of metal-halide lamps would be interesting.

Substantial axial segregation of Dy is also apparent in figure 6.10. The Dy mixing ratio is at least a factor of three lower at the midplane of the lamp than at the bottom. The Fischer segregation parameter characterizing axial segregation was determined by least squares fit (see figure 6.12). A weighted average over all radial positions gives $\lambda_{\{Dy\}} = 0.215 \pm 0.002 \text{ mm}^{-1}$. This result is 7% larger than the $\lambda_{\{Dy\}} = 0.20 \pm 0.01 \text{ mm}^{-1}$ found by Flikweert *et al* [6] using laser-absorption.

Radial segregation of I is practically non-existent. As discussed in Section 6.2, theory suggests there should not be a rapid change in the I mixing ratio across the transition region where DyI_3 is dissociated. In addition, I has an ionization energy slightly higher than Hg and much higher than Dy. The fractional ionization of I is very low, even in the core of the arc. Therefore, the ambipolar term for Dy that leads to equation 6.14 is negligible for I. The simplified theoretical picture of Section 6.2 does not suggest any radial segregation for I.

The absence of significant radial segregation for I, in turn, limits axial segregation of I. The Fischer axial segregation parameter for I, a weighted average over all radial positions, was found to be $\lambda_{\{I\}} = 0.056 \pm 0.001 \text{ mm}^{-1}$. This is a factor of 4 less than for the axial segregation parameter for Dy.

6.5 Conclusions

Absolute elemental densities of Dy and Hg have been obtained in a metal-halide lamp as a function of radial and axial location using x-ray induced fluorescence. The mixing ratio $n_{\{Dy\}}/n_{\{Hg\}}$ shows significant axial and radial segregation of Dy. The Fischer segregation parameter for Dy, averaged over radial position, is determined to be $\lambda_{\{Dy\}} = 0.215 \pm 0.002 \text{ mm}^{-1}$. Both Dy density and Fischer parameter are in agreement with laser absorption measurements done by Flikweert *et al* [6] where neutral atomic Dy densities were measured. An excess of I in the gas phase is created as Dy reacts with the burner wall and forms Dy silicates. I shows less radial and axial segregation than Dy, in agreement with theory. The axial segregation parameter for I, averaged over radial position, is $\lambda_{\{I\}} = 0.056 \pm 0.001 \text{ mm}^{-1}$. This is 4 times less than for Dy.

A simplified theoretical description of radial fluxes is partially successful in describing the measured mixing ratios and earlier observations of optical emission.

6.6 Acknowledgements

Use of the Advanced Photon Source was supported by the U. S. Department of Energy, Office of Science, Office of Basic Energy Sciences, under Contract No. DE-AC02-06CH11357. The authors thank M.L. Beks and A. Hartgers for theoretical discussions. T.N. acknowledges support from Technologiestichting STW (project ETF. 6093).

Bibliography

- [1] Lister G G, Lawler J E, Lapatovich W P and Godyak V A 2004 *Rev. Mod. Phys.* **76**, 541
- [2] Fischer E 1976 *J. Appl. Phys.* **47**, 2954
- [3] Curry J J, Adler H G, Shastri S D, Lee W -K 2003 *J. Appl. Phys.* **93**, 2359
- [4] Curry J J, Adler H G, Shastri S D, J.E. Lawler 2001 *Appl. Phys. Lett.* **79**, 1974
- [5] Nimalasuriya T, Pupat N B M, Flikweert A J, Stoffels W W, Haverlag M and Van der Mullen J J A M 2006 *J. Appl. Phys.* **99** 053302 **see chapter 2**
- [6] Flikweert A J, Nimalasuriya T, Groothuis C H J M, Kroesen G M W and Stoffels W W 2005, *J. Appl. Phys.* **98** 073301
- [7] Nimalasuriya T, Flikweert A J, Haverlag M, Van der Mullen J J A M, Kemps P C M, Kroesen G M W, Stoffels W W, Van der Mullen J J A M 2006 *J. Phys D: Appl Phys* **39** 2993 **see chapter 3**
- [8] Flikweert A J, Van Kemenade M, Nimalasuriya T, Haverlag M, Kroesen G M W and Stoffels W W 2006 *J.Phys.D* **39**, 1599
- [9] Nimalasuriya T, Thubé G M, Flikweert A J, Haverlag M, Kroesen G M W, Stoffels W W, Van der Mullen 2007, *J.Phys.D* 2007 **40** 2839, **see chapter 4**
- [10] Kroesen G M W, Haverlag M, Dekkers E, Moerel J, de Kluijver R, Brinkgreve P, Groothuis C H J M, Van der Mullen J J A M, Stoffels W W, Keijser R, Bax M, Van den Akker D, Schiffeleers G, Kemps P C M, Van den Hout F H J, Kuipers A 2005 *Microgravity sci. technol.* XVI-1
- [11] Stoffels W W, Haverlag M, Kemps P C M, Beckers J and Kroesen G M W 2005 *Appl. Phys. Lett.* **87** 1
- [12] Zhu X 2005 Ph.D. thesis, Eindhoven University of Technology
- [13] Raizer Y P, 1991 *Gas Discharge Physics*, 1st ed., (Springer verlag).
- [14] Hartgers A, Van der Heijden H W P, Beks M L, Van Dijk J, Van der Mullen J J A M 2005 *J. Phys D: Appl Phys*, **38** 3422-29, equation (36)
- [15] Stoffels W W, Flikweert A J, Nimalasuriya T, Van der Mullen J J A M, Kroesen G M W, Haverlag M, 2006 *Pure Appl. Chem.* **78** No 6
- [16] <http://www.aps.anl.gov/>
- [17] Elenbaas W 1951 *The high pressure mercury vapour discharge*, 1st ed., (North-Holland publishing company)

Chapter 6.

- [18] Kenty C 1938 J. Appl. Phys. **9**
- [19] Van der Mullen J J A M 1990 Phys. Rep. **191** 109
- [20] <http://www.csrri.iit.edu/>